Tailoring the interaction between spin waves and domain walls in nanostripes with perpendicular magnetic anisotropy

Rocio Yanes[1], Nerea Ontoso[2], Luis Torres[1] and Luis Lopez-Diaz[1]

[1]*Department of Applied Physics, University of Salamanca, Spain*
[2]*CIC nanoGUNE, 20018 Donostia-San Sebastian, Basque Country, Spain*

We study the interaction between spin waves and domain walls in perpendicularly magnetized nanostripes in presence of a uniform in-plane field and how such field can be used to modulate the domain wall velocity and the spin wave phase that result from this interaction. On one hand, the external field is found to enhance the excitation of an internal non-uniform flexural mode at specific frequencies, which can lead to an increase by a factor of six in the domain wall velocity. On the other, in a lower frequency regime, the field orientation modulates the DW reflectivity yielding higher velocities when the field is applied along the nanostripe width. Finally, a linear relation of slope two is found between the in-plane field angle and the spin wave phase.

Spin waves (SWs) are small unlocalized perturbations of the magnetic order in the form of a phase-coherent precession of the magnetic moments, whereas domain walls (DWs) are regions where the magnetization direction changes rapidly with a well defined size and profile. Despite of their very different nature, both SWs and DWs occur naturally in materials with ferromagnetic order and both the knowledge and the ability to manipulate them at the nanoscale have grown substantially over the last years, which have led to interesting phenomena relating the interaction between them. For example, it has been found that pinned DWs can emit coherent SWs when they oscillate around the equilibrium position[1, 2] or release energy in the form of incoherent SWs as they propagate in a medium with disorder[3, 4]. On the other hand, DWs can channel SW propagation along them acting as efficient waveguides[5, 6]. They can also induce a phase- shift in the SWs [7] as they pass across and, furthermore, this phase shift can be dependent on the DW chirality in systems with suitable Dzyaloshinkii-Moriya interaction (DMI) and dimensions[8]. This is interesting for the development of magnonic devices that could possibly use SW phase for data storage and processing. Other methods have been proposed to control SW phase, such as using switchable nanomagnets on top of the wave guide[9], dipolarly coupled dot arrays with reconfigurable point defects[10], or passing a moderate current through the device[11]. With newly developed techniques [12] SW phase can now be resolved experimentally and the search for practical schemes to manipulate it continues.

Reciprocally, it has been predicted theoretically that propagating SWs can move DWs when they run into them, in both in-plane [13–17] and perpendicularly magnetized [18–20] systems. Experimentally, it has been shown that colliding DWs release energetic SW bursts that can assist depinning of a nearby DW[21]. Nevertheless, direct experimental evidence of DW motion induced by coherent SWs is still a challenge, mostly because in metallic ferromagnets SW attenuate rapidly as they move away from the source. Recent fabrication of FeCo alloys with ultra-low damping[22], however, allows for hope to be able to use SW as an efficient way to displace DWs in a controllable manner.

From the theoretical studies carried out so far it is already well known that SWs can move DWs in either negative direction (opposite to SW flow) or positive one (same than SW flow), depending on whether the dominant mechanism is transfer angular momentum to the DW as they pass through [14, 23], or linear momentum as they are reflected [18]. A third mechanism has been identified, namely SW excitation of an internal DW oscillatory mode [13, 19, 20], involving transfer of linear momentum to the DW and, therefore, positive velocity. Although some reduced models have been developed to describe SW assisted DW motion considering the DW as a rigid object[17, 18], the theoretical investigation of this last mechanism relies entirely on micromagnetic simulations, since energy absorption of the DW cannot be accounted for within such reduced models. The different mechanisms involved make SW assisted DW motion an attractive approach for its flexibility, since it allows selecting the direction in which the DW moves and its velocity being controlled with the amplitude of the SWs. However, the preponderance of one particular mechanism over the others in a given situation is hard to know a priori, since it depends non trivially on the SW frequency, the internal profile of the magnetic DW[24], the relation between the SW length and the DW width[25], the lateral size of the system[19] or the existence of sizeable DMI[26, 27]. The understanding of SW assisted DW motion is, therefore, still incomplete and a practical method to manipulate DW motion with SWs is lacking.

In this work we present a simple scheme to achieve a flexible control of the interaction between DWs and SWs in ferromagnetic nanostripes with high perpendicular magnetic anisotropy (PMA). It is based on the application of a small in-plane field which, by means of carefully chosen dimensions, allows to easily change the

internal profile of the DW and, consequently, the way it interacts with the incoming SWs.

The spatial and time evolution of the magnetization in the system is obtained by numerically solving the Landau-Lifshitz-Gilbert equation taking into account exchange, magnetostatic, magnetocrystalline anisotropy and Zeeman interactions. A computational region of dimensions $L_x \times L_y \times L_z = 10000 \times 64 \times 1.5$ nm^3 is considered, as shown in the top of Fig. 1(a). Micromagnetic simulations were performed using the GPU-based software package MuMax3[28] with $2 \times 2 \times 1.5$ nm^3 cell size. The following material parameter values, typical of CoFeB, are used: exchange stiffness $A = 1.3 \times 10^{-11}$ J/m, saturation magnetization $M_s = 8.6 \times 10^5$ A/m, PMA constant $K_z = 5.8 \times 10^5$ J/m^3 and Gilbert damping constant $\alpha = 0.015$.

A DW separating two antiparallel domains is placed at the center of the computational region ($x = 0$, inset of Fig. 1(a)). The nanowire width ($L_y = 64$ nm) is chosen so that the energy difference between the Bloch and Néel configurations is small and, therefore, its in-plane orientation is sensitive to a small external field. The profile of the stabilized DW for our dimensions without any applied field is not pure Néel nor Bloch type, but an intermediate one [19]. The application of a in-plane field does not induce a net displacement of the DW but, as it will be shown, it modifies its internal profile and, consequently, its interaction with SWs. The SWs are excited by means of a localized AC magnetic field with a Gaussian profile, $\vec{B}_{AC}(x,t) = B_{AC} \exp\left[-(x-x_0)^2/\sigma^2\right] \sin(2\pi\nu t)\,\hat{y}$, with $x_0 = -1\,\mu$m and $\sigma = 20$ nm. A smooth profile is chosen because, as pointed out recently, abrupt "square box" profiles might introduce spurious effects in the frequency dependence of the magnonic torque [29]. On the other hand, the distance between the DW and the SW source ($1\,\mu$m) guarantees that the interaction between SWs reflected by the DW and the SW source is negligible. Finally, the amplitude of the field is kept below $B_{AC} = 90$ mT with the aim of using realistic values and minimizing non-linear effects.

First, we investigate the dynamics of a DW induced by SWs under an in-plane static field B_{DC} along both the longitudinal (x) and transverse (y) axis of the nanostripe. Different amplitudes of B_{DC} have been considered up to a maximum of 20 mT. The average velocity of the DW in a given time interval Δt is calculated from the variation of averaged z component of the nanostripe magnetization, $<m_z>$, as $V_{DW} = \frac{\Delta <m_z>}{\Delta t}\frac{L_x}{2}$. Our simulations show that the transient period until the steady motion of the DW is reached can extend up several tens of nanoseconds. Therefore, the DW velocity is computed only from the last 5 ns of the total simulation time $t_{sim} = 50$ ns.

In Fig. 1(a) we compare the calculated DW velocity as a function of the SW frequency without static field with the ones calculated considering an in-plane field of $B_{DC} = 16$ mT along the x and y axis, whereas in the
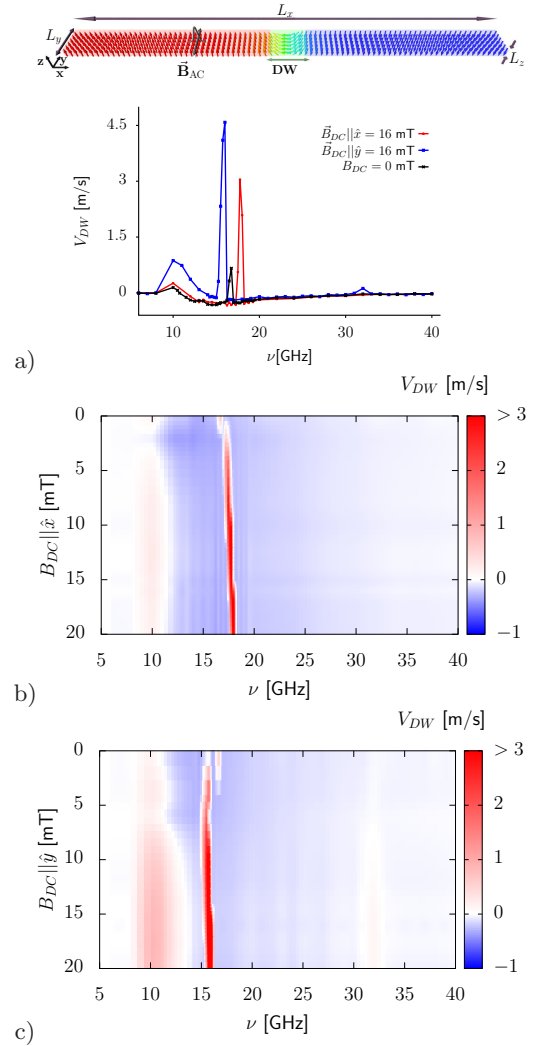
Figure 1. (a) Frequency dependence of DW velocity for $B_{DC} = 0$ (black), $\vec{B}_{DC} = 16\,\mathrm{mT}\,||\,\hat{x}$ (red) and $\vec{B}_{DC} = 16\,\mathrm{mT}\,||\,\hat{y}$ (blue). Schematic representation of the system under study on the top. (b) and (c) DW velocity as a function of SW frequency and field amplitude for a field applied along the x and y directions, respectively.

lower panels we present 2D plots of the DW velocity as a function of the frequency and the applied field amplitude B_{DC} along both x (b) and y (c) axis.

Some general trends in the frequency dependence of V_{DW} can be identified. No effect on the DW is obtained below 8 GHz simply because in this range SWs do not propagate ($\nu_{\mathrm{FMR}} \approx 8$ GHz). Right above this threshold we observe a region of positive velocity, which can be explained taking into account that in this region the wavelength of the SWs is larger than the DW width and, therefore, they are mostly reflected by the DW. Consequently, there is a transfer of linear momentum from the SWs to the DW that pushes the latter away from the SW source. As the excitation frequency increases ($\nu \sim 11-30$ GHz) the wavelength decreases and SW transmission is
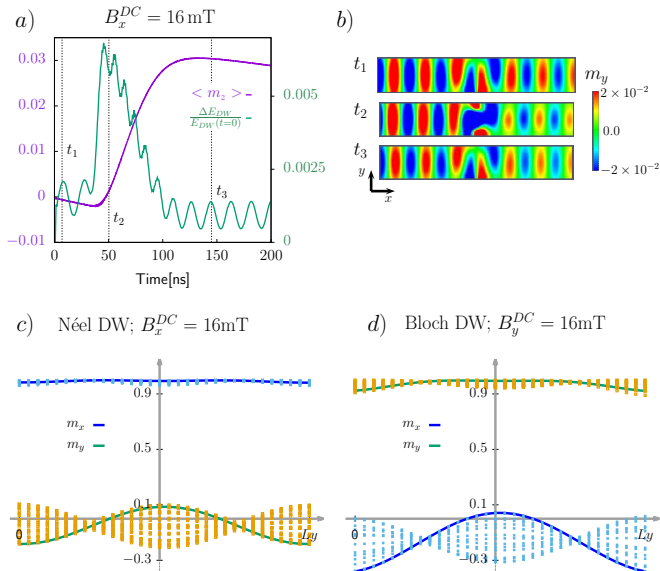
Figure 2. (a) Time evolution of $< m_z >$ and the normalized increment of DW energy with $\nu = 18\,$GHz and $\vec{B}_{DC} = 16\,$mT $\hat{x}$. (b) Snapshots of m_y at $t = 7$, 50.25 and 145 ns. (c),(d) Transverse profile of m_x and m_y at the center of the DW for (c) $\nu = 18.0\,$GHz and $\vec{B}_{DC} = 16\,$mT $\hat{x}$ and (d) $\nu = 16.0\,$GHz and $\vec{B}_{DC} = 16\,$mT $\hat{y}$. Profiles at different time instants are plotted with points and the one with maximum amplitude is highlighted with a line.

favored, entailing transfer of angular momentum between the SW and DW, which leads to the DW motion towards the SW source (negative velocity). At larger frequencies ($\nu > 30$ GHz), SWs decay rapidly and their amplitude is negligible when they reach the DW, being incapable of moving it. Interestingly, the DW velocity displays a pronounced peak around 16.75 GHz (in the $B_{DC} = 0$ case) which, as it will be shown later, is related to the activation of an internal mode of the DW.

On the other hand, it is observed that the application of an in-plane field has a significant impact on DW velocity. It was shown by Chang et al. [20] that the application of this field increases the DW rigidity, which favours SW reflection and hinders transmission across the DW. This is corroborated by our simulations, which show an increase in the positive velocity at low frequencies, more pronounced in the Bloch wall case ($\vec{B}_{DC} || \hat{y}$), and a reduction of the negative one in the transmission regime. Additionally, we notice that the static field increases the DW speed when the internal modes of the DW are excited, reaching velocities close to 5 m/s.

Let us focus our attention on investigating the process that leads to the sharp peaks in the velocity highlighted before (Fig. 1). Several computational works[13, 17, 19] relate similar peaks to the excitation of an internal mode of the DW. To confirm it, in Fig. 2(a) we plot the time evolution of $< m_z >$ together with the normalized increment of DW energy with respect to its value at rest,

$\Delta E_{DW} = E_{DW}(t) - E_{DW}(t = 0)$, for an applied field $B_{DC} = 16$ mT along the x axis. As it can be observed, at $t = 38.2\,$ns the change in the dynamic regime is linked to a rapid increment of the DW energy. This increment is related to the DW changing its internal profile, as evidenced in Fig. 2(b), where we compare the space distribution of m_y around the DW center at three time instants corresponding to each one of the three dynamic regimes identified. As can be observed, in the excited regime m_y is not uniform across the wall and the DW itself displays some flexural distortion[30] (supplementary material). It is also apparent that the intensity of the SWs is substantially reduced to the right of the DW in the second regime ($t_2 = 50.25\,$ns) which, together with Fig. 2(a), indicates that the DW absorbs a significant amount of energy from the incident SWs. As the DW moves away from the source the amplitude of the SWs decreases and the internal mode is eventually deactivated. The DW recovers its quasi-uniform profile and negative velocity, the latter smaller than in regime 1 due to the lower SW amplitude. The nature of the internal DW excitation is illustrated in Fig. 2(c,d), where we show the profile along the nanostripe width of the magnetization in-plane components inside the DW for a field of 16 mT applied along the x (c) and y (d) axis. It is evident that in the excited mode the central part and the edges of the DW oscillate out of phase. In each case it is the in-plane component transversal to the DW that oscillates, m_y for the Néel wall (Fig. 2(c)) and m_x for the Bloch wall (Fig. 2(d)). The frequency of the Bloch wall internal excitation is slightly lower than Néel one (Fig. 1), in agreement with a recent theory for DW flexural dynamics in perpendicularly magnetized media[30].

As mentioned before, without applied field ($B_{DC} = 0$) the DW is not pure Néel nor Bloch type, and therefore, both m_x and m_y oscillate with similar amplitude (supplementary material) when excited at the appropriate frequency (16.75 GHz), intermediate between the Bloch ($\nu \sim 16$ GHz) and Néel ($\nu \sim 18$ GHz) characteristic frequencies (see Fig. 1). When the field B_{DC} is applied along either x or y axis, the DW acquires a well defined Néel or Bloch profile, respectively. Despite of being uniform in space, it seems that B_{DC} promotes the excitation of the non-uniform internal DW mode, as evidenced by the increase of V_{DW} with B_{DC} observed in Fig. 1(b) and (c). To explain this, we point out that the dominant component of the torque exerted by B_{DC} on the DW, (τ_{DC}^{DW}), is proportional to its transversal component (supplementary material). Therefore, the non-uniformity in the transversal component induced by the SW excitation (Fig. 2(b)) yields a non-uniform torque that further enhances the amplitude of the flexural mode of the DW.

Continuing with our study, we investigate SW induced DW dynamics as a function of the in-plane orientation of the applied field. The amplitude of the field is kept constant, $B_{DC} = 16$ mT, whereas the in-plane orienta-
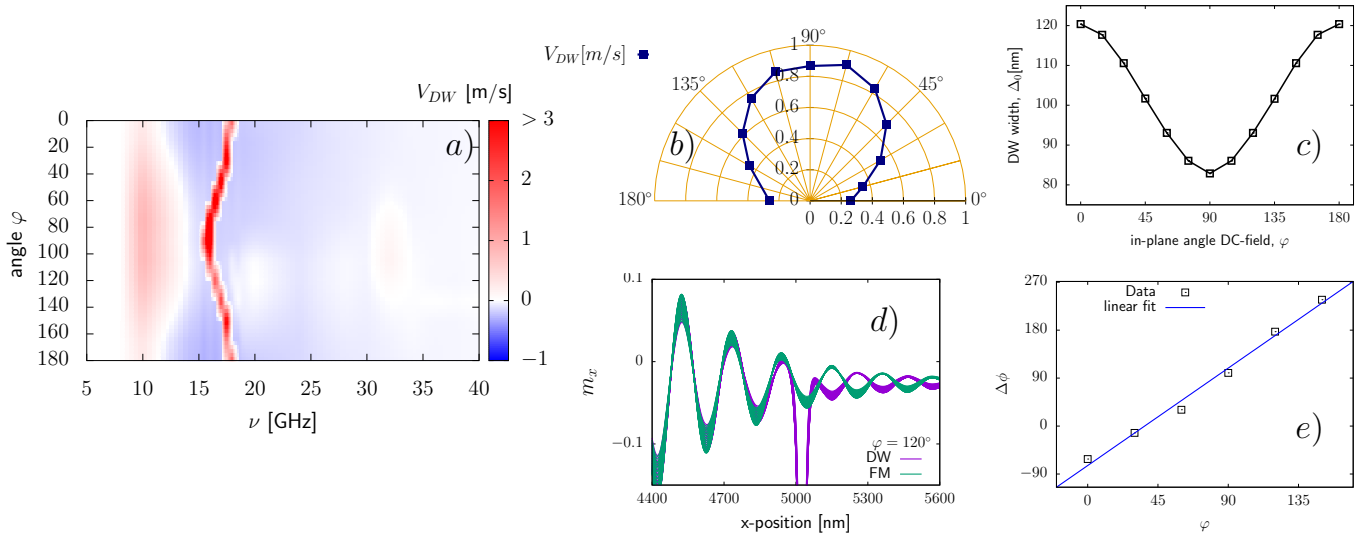
Figure 3. For $B_{DC} = 16$ mT: (a) DW velocity as a function of the SW frequency, ν, and the field angle φ. For SW frequency, $\nu = 10$ GHz: (b) Polar plot of DW velocity versus in-plane field angle φ. (c) Computed DW width at equilibrium, Δ_0, as a function of in-plane field angle φ. (d) Profile of m_x at the center of the nanostripe with (purple) and without (green) DW, for $\varphi = 120°$ and at the same time instant ($t = 45$ ns). (e) DW induced phase shift $\Delta\phi$ as a function of in-plane field angle φ.

tion φ, $B_{DC} = B_{DC}(\cos\varphi, \sin\varphi, 0)$, is swept in the range $0° < \varphi < 180°$. The computed DW velocity values as a function of both SW frequency and angle φ are plotted in Fig. 3(a). Similarly to the results presented in Fig. 1(b-c), for most of the allowed SW frequencies the DW velocity is small ($|V_{DW}| < 0.25$ m/s) and negative as a consequence of the SW transferring angular momentum to the DW when passing through. The narrow region of large positive velocity corresponding to the excitation of the internal DW mode is symmetric with respect to $\varphi = 90°$ and gradually shifts between the two extreme values, $\varphi = 90°$ (Bloch wall) and $\varphi = 0°, 180°$ (Néel wall), discussed before (see Fig. 1(b) and (c)).

On the other hand, a region of moderate positive velocities for frequencies just above the propagation threshold (8-12 GHz) is also present. This region notoriously broadens as the field is rotated towards the y axis (Fig. 3(a)) and also the DW velocities are higher, as shown in Fig. 3(b), where the computed DW velocities for a SW excitation of $\nu = 10$ GHz and different in-plane orientations are shown in a polar plot. To explain this one has to keep in mind that, as mentioned before, the positive velocity in this region is due to the fact that SW wavelength is larger than DW width and, consequently, transfer of linear momentum of the reflected SWs is the dominant mechanism that moves the DW. As can be observed in Fig. 3(c), the DW width decreases as the field is rotated towards the y axis, reaching a minimum for the Bloch wall. This DW width reduction increases the DW reflectivity, leading to higher positives velocities and to the extension of this behaviour towards higher frequencies (smaller wavelengths).

On the other hand, and changing the perspective from

SW induced DW motion to the effect of the DW on the SWs that pass through it, in Fig. 3(d) we compare the profile of m_x along the central area of nanostripe of a SW propagating with and without the presence of a DW. It is apparent from this comparison that the DW introduces a phase shift in the SW. This phase shift $\Delta\phi$ is computed for each applied field orientation and the results are shown in Fig. 3(e). As can be observed, a linear dependence $\Delta\phi = 2\varphi - \frac{\pi}{2}$ is obtained for the whole range, proving that an orientable in-plane field allows us to modify the SW phase in a controllable way, a finding that future magnonic applications could make use of.

In summary, we presented a easy way to control the interaction between DWs and SWs in nanostripes with high PMA using an small in-plane field. On one hand, this field enhances the excitation of an internal DW oscillatory mode at specific frequencies, which permits higher DW velocities. On the other, in the low frequency regime, we show that the field in-plane orientation modulates the DW reflectivity. Finally, we find that field orientation can be also used to reliably modify the SW phase over the whole 2π range, which could be considered as a realization of a linear SW phase shifter.

See supplementary material for (1) animation of flexural mode and (2) amplification of the flexural mode by an in-plane field.

[1] B. Van de Wiele, S. J. Hmlinen, P. Bal, F. Montoncello, and S. van Dijken, Scientific Reports **6**, 21330 (2016).

[2] M. Voto, L. Lopez-Diaz, and E. Martinez, Scientific Reports **7**, 13559 (2017).

[3] H. Min, R. D. McMichael, M. J. Donahue, J. Miltat, and M. D. Stiles, Phys. Rev. Lett. **104**, 217201 (2010).

[4] M. Voto, L. Lopez-Diaz, and L. Torres, J. Phys. D: Appl. Phys. **49**, 185001 (2016).

[5] K. Wagner, A. Kkay, K. Schultheiss, A. Henschke, T. Sebastian, and H. Schultheiss, Nat Nano **11**, 432 (2016).

[6] F. Garcia-Sanchez, P. Borys, R. Soucaille, J.-P. Adam, R. L. Stamps, and J.-V. Kim, Phys. Rev. Lett. **114**, 247206 (2015).

[7] R. Hertel, W. Wulfhekel, and J. Kirschner, Phys. Rev. Lett. **93**, 257202 (2004).

[8] F. Buijnsters, Y. Ferreiros, A. Fasolino, and M. Katsnelson, Phys. Rev. Lett. **116**, 147204 (2016).

[9] Y. Au, M. Dvornik, O. Dmytriiev, and V. V. Kruglyak, Appl. Phys. Lett. **100**, 172408 (2012).

[10] S. Louis, I. Lisenkov, S. Nikitov, V. Tyberkevych, and A. Slavin, AIP Advances **6**, 065103 (2016).

[11] V. E. Demidov, S. Urazhdin, and S. O. Demokritov, Appl. Phys. Lett. **95**, 262509 (2009).

[12] Y. Hashimoto, T. H. Johansen, and E. Saitoh, Appl. Phys. Lett. **112**, 072410 (2018).

[13] D.-S. Han, S.-K. Kim, J.-Y. Lee, S. J. Hermsdoerfer, H. Schultheiss, B. Leven, and B. Hillebrands, Appl. Phys. Lett. **94**, 112502 (2009).

[14] P. Yan, X. S. Wang, and X. R. Wang, Phys. Rev. Lett. **107**, 177207 (2011).

[15] J.-S. Kim, M. Strk, M. Klui, J. Yoon, C.-Y. You, L. Lopez-Diaz, and E. Martinez, Phys. Rev. B **85**, 174428 (2012).

[16] P. Yan, A. Kamra, Y. Cao, and G. E. W. Bauer, Phys. Rev. B **88**, 144413 (2013).

[17] X.-G. Wang, G.-H. Guo, G.-F. Zhang, Y.-Z. Nie, and Q.-L. Xia, Journal of Applied Physics **113**, 213904 (2013).

[18] X.-g. Wang, G.-h. Guo, Y.-z. Nie, G.-f. Zhang, and Z.-x. Li, Phys. Rev. B **86**, 054445 (2012).

[19] H. Hata, T. Taniguchi, H.-W. Lee, T. Moriyama, and T. Ono, Appl. Phys. Express **7**, 033001 (2014).

[20] L.-J. Chang, Y.-F. Liu, M.-Y. Kao, L.-Z. Tsai, J.-Z. Liang, and S.-F. Lee, Scientific Reports **8**, 3910 (2018).

[21] S. Woo, T. Delaney, and G. S. D. Beach, Nat Phys **13**, 448 (2017).

[22] M. A. W. Schoen, D. Thonig, M. L. Schneider, T. J. Silva, H. T. Nembach, O. Eriksson, O. Karis, and J. M. Shaw, Nature Physics **12**, 839 (2016).

[23] D. Hinzke and U. Nowak, Phys. Rev. Lett. **107**, 027205 (2011).

[24] S.-M. Seo, H.-W. Lee, H. Kohno, and K.-J. Lee, Appl. Phys. Lett. **98**, 012514 (2011).

[25] S. Macke and D. Goll, J. Phys.: Conf. Ser. **200**, 042015 (2010).

[26] W. Wang, M. Albert, M. Beg, M.-A. Bisotti, D. Chernyshenko, D. Corts-Ortuo, I. Hawke, and H. Fangohr, Phys. Rev. Lett. **114**, 087203 (2015).

[27] P. Borys, F. Garcia-Sanchez, J.-V. Kim, and R. L. Stamps, Adv. Electron. Mater. **2**, n/a (2016).

[28] A. Vansteenkiste, J. Leliaert, M. Dvornik, M. Helsen, F. Garcia-Sanchez, and B. Van Waeyenberge, AIP Advances **4**, 107133 (2014).

[29] V. Risinggrd, E. G. Tveten, A. Brataas, and J. Linder, Phys. Rev. B **96**, 174441 (2017).

[30] R. Soucaille, F. Garcia-Sanchez, J.-V. Kim, T. Devolder, and J.-P. Adam, Phys. Rev. B **98**, 054426 (2018).